In vivo quantification of human lung dose response relationship

Walter O'Dell [*ab], Peng Wang [a], Haisong Liu[b], David Fuller[b], Michael C. Schell[ab], Paul Okunieff[b]

[a] Department of Biomedical Engineering, University of Rochester, Rochester, NY, USA 14642
[b] Department of Radiation Oncology, University of Rochester, Rochester, NY, USA 14642

ABSTRACT

Purpose: To implement a new non-invasive *in-vivo* assay to compute the dose-response relationship following radiation-induced injury to normal lung tissue, using computed tomography (CT) scans of the chest.
Methods and Materials: Follow-up volumetric CT scans were acquired in patients with metastatic tumors to the lung treated using stereotactic radiation therapy. The images reveal a focal region of fibrosis corresponding to the high-dose region and no observable long-term damage in distant sites. For each pixel in the follow-up image the treatment dose and the change in apparent tissue density was compiled. For each of 12 pre-selected dose levels the average pixel tissue density change was computed and fit to a two-parameter dose-response model. The sensitivity of the resulting fits to registration error was also quantified.
Results: Complete *in vivo* dose-response relationships in human normal lung tissue were computed. Increasing radiation sensitivity was found with larger treatment volume. Radiation sensitivity increased also over time up to 12 months, but decreased at later time points. The time-course of dose response correlated with the time-course of levels of circulating IL-1α, TGFβ and MCP-1. The method was found to be robust to registration errors up to 3 mm.
Conclusions: This approach for the first time enables the quantification of the full range dose response relationship in human subjects. The method may be used to assess quantitatively the efficacy of various agents thought to illicit radiation protection to the lung.

Keywords: Lung cancer treatment, stereotactic radiotherapy, computed tomography, radiation dose-response, radioprotectors

1. INTRODUCTION

1.1 Current clinical perspective

The aim of this study is to demonstrate a new non-invasive *in vivo* assay for quantifying the response of normal lung tissue to radiation injury. The lung is a very radiosensitive organ and damage to the lung is an unavoidable complication of thoracic irradiation. As such, concern for radiation toxicity to the lungs often limits the dose delivered, in many cases reducing the expectation of treatment from curative to palliative. At present, the delivery of inhomogeneous doses to very focal volumes containing normal tissue has as yet unknown long-term sequelae. The issues of tolerance are particularly important for those organs that are commonly host to lethal metastases.

Recent clinical studies performed at the Authors' institution indicate that when curative doses are applied, hypofractionated, conformal, high-dose stereotactic radiation therapy in the lung can achieve a greater than 90% local control rate and provide significant improvement in patient long-term survival[1]. Of primary breast cancer patients who presented with 5 or fewer lung metastases, 36% were deemed to be disease free at 40-months post-treatment[1]. Moreover, no overall clinical IV toxicity was observed (based on the 5-level RTOG scale), only one occurrence (out of 50 patients) of grade III toxicity (non-malignant pleural effusion), and overall grade II toxicity was limited to cough. In contrast to conventional radiation treatment where a near-uniform dose is delivered to a large volume, pulmonary stereotactic radiotherapy (PSRT) delivers a well-defined heterogeneous dose with a large penumbra to a small lung region. A slice through a representative treatment plan for an isolated lung metastasis is shown in Figure 1. PSRT provides a unique environment in which to study the response of normal tissue to radiation. First, PSRT imparts greatly varying dose values

* wodell@rochester.edu; phone 1 585 273-4103; http://radonc.urmc.rochester.edu/~wodell/

(from near zero to over 50 Gy) in the neighborhood of each lesion with almost no radiation to distal sites within the same organ. These features enable the determination of full-range dose-response curves for the normal tissue around each individual lesion in each patient. Second, because many patients present with multiple lung lesions the effect of the local irradiated volume on the local dose-response relationship can be investigated within the same patient. This provides an intrinsic control for contributing factors including age, smoking history, genetic disposition, circulating cytokine levels, etc. Third, complete image sets are available over the course of treatment and at multiple time points post-therapy, providing the ability to monitor the time course of the tissue response. Fourth, the treatment volumes are sufficiently small that systemic reaction to the radiation insult is believed to be absent, removing from play secondary moderating effects such as radiation-induced elevation of circulating cytokine levels. Fifth, the treatment sites are often sufficiently small and sufficiently separated from each other and from surrounding structures (such as the chest wall, heart, and large vessels) to be reliably distinguished and their effects isolated and studied individually. Finally, with the use of lethal radiation doses at the target site there is no residual tumor mass observed > 3 months post-treatment, thereby eliminating the possibility that residual tumor mass may corrupt the response analysis at time points greater than or equal to 3 months. The extended survival of these PSRT patients[1] also enables the study of radiation late-effects at very long time points.

The utility of a non-invasive *in vivo* dose response assay is three-fold. First, it could be used to quantify the efficacy of both preventive and palliative agents used to moderate radiation-induced injury in normal tissue, thereby helping to bring new drugs and interventions more rapidly to market. Second, because it is applicable to both human subjects and animal models it could be used to correlate bench-top results with clinical endpoints of physiologic response. Third, it is hoped that through these attributes it will ultimately lead to improvements in our understanding of the radiobiology of lung tissue.

1.2 Underlying radiobiology

In the lung, acute radiation effects of cellular injury, DNA damage and apoptosis give way to an early inflammatory response at the tissue level and into chronic late-effects of progressive tissue fibrosis and pneumonitis that take precedence 3-6 months post-radiation therapy and appear to escalate throughout the patient's life. The symptomatic results are increasing dyspnea ("breathlessness") that can progress to hypoxemia and death. The acute and early responses are fairly well understood on the cellular and tissue levels[2], but the same cannot be said of very long-term (> 6-months) effects in humans. The severity of the local toxicity has long been assumed to be entirely a function of the radiation dose and the volume of lung irradiated, yet the classic models do not explain the substantial inter-patient variability of response[3]. The roles played by autoimmune disease, chemotherapy, infection, and trauma are also well appreciated but not well explained. Recent clinical and experimental studies indicate that the development of radiation-induced fibrosis may be dependent on the baseline circulating levels of some cytokines[4-6]. However, this and related hypotheses heretofore have not been confirmed quantitatively in human subjects because we have lacked the means to quantify dose response reactions of lung tissue *in vivo* in patients with long term survival following high-dose radiation therapy[7].

In this study, we demonstrate a volumetric computed tomography (CT) imaging-based assay for radiation sensitivity of tissue. The method is applied to patients treated at our institution for isolated lung lesions using PSRT. Our hypothesis is that our method can be used to quantify differences in the radiobiologic response of normal lung tissue sufficient for discerning changes in response due to the effects of measurable alterations in moderating co-factors such as treatment volume, treatment time and circulating cytokines.

2. METHODS

2.1 Patient selection and treatment

Human dose response datasets were obtained at our institution from two patients being treated for one or more lung metastases. All protocols were approved by our institutional review board and all patients were given informed consent as per institutional and federal guidelines for the use of human subjects in research. Patient #1 was treated for 5 isolated lung metastases, ranging in size from 8-14 mm in diameter. Patient #2 was treated for a solitary tumor of 18 mm in diameter. All lesions were treated using a fractionation schedule of 10 fractions of 5 Gy/fraction with high-energy X-ray beams directed along multiple trajectories. Reflective surface markers on the chest and abdomen and individually-shaped vacuum bags were used for all CT image acquisitions and radiation treatments to improve the reproducibility of

positioning between planning CT scans and the daily fractionated treatments[8]. Radiation exposure was performed during periods of end-expiration breath hold, using the surface marker positions as a guide, as detailed in references[1, 9]. Under the clinical protocols we obtained pretreatment planning CT image datasets, pretreatment dose distribution calculations, and 6, 12, 18 and 24 month follow-up CT images.

2.2 Dose calculation

The 3D dose distributions were computed in a ~10× 10× 10 cm region centered at each target using commercial treatment planning system software (BrainScan 5.1 from BrainLAB AG, Heimstetten, Germany). The overall dose sampling size was chosen to encompass the entirety of the 20% isodose line (~10 Gy), and include much of the 10% and lower dose regions (Figure 1). The dose sampling density and spacing was prescribed to match the location and size of the pretreatment planning CT image voxels. The volumetric dose was, by the choice of sampling locations during computation, aligned precisely with the pretreatment planning CT dataset.

2.3 CT image acquisition

The image data was obtained using a commercial, clinical CT scanner (GE Genesis Lightspeed CT scanner, GE medical system, Milwaukee, Wisconsin) and with imaging parameters consistent with standard-of-care follow-up images at the Authors' institution. These parameters were an in-plane pixel size of 0.94 mm; slice thickness and slice separation of 3mm; tube voltage of 120 kVp; and tube current of 250 mA.

2.4 Lung segmentation

To exclude from the analysis image pixels corresponding to surrounding anatomical structures, such as the chest wall, heart and diaphragm, an automatic lung segmentation algorithm was applied that incorporated standard histogram-based thresholding and morphological image operations. This step allowed the registration task to be driven entirely by pixels within the lung volume, resulting in a faster computation that was less dependent on extra-pulmonary tissues such as the skin layer whose composition can be expected to undergo measurable change during the 6- and 12- month lapse between image acquisitions. For these initial studies, manual rigid body registration method was applied to the target sites in the segmented hemi-lung of interest to align the post-treatment image datasets to the planning CT dataset.

2.5 Image registration and data analysis

The end-point of the analysis was to obtain plots of radiation dose exposure versus change in observable CT Hounsfield units (HU) at various time-points post-therapy. Following the lung volume extraction and registration steps, the procedure was to then collect at each pixel in the 3D image set the change in CT image intensity (in Hounsfield units) and the prescribed radiation dose applied during treatment. To filter out excessive noise and variance in the dose data, the dose values were binned into 5Gy-wide bins and the average CT intensity change was computed over all pixels within each bin. For the analyses shown in Figures 2-5, the baseline CT Hounsfield value was computed as the average CT intensity value within a ~1 cm^2 rectangular region drawn in the vicinity of each treatment site at the CT image slice passing through the center of the tumor. The change in CT intensity at each pixel was computed as the difference between the intensity in each pixel in the follow-up image and the baseline intensity value. This baseline subtraction, individualized for each target site, ensured that the starting dose-response data (that at very low doses) was uniformly zero-valued for each target site. For each treatment site, the data was normalized to the maximum measured radiation-induced Hounsfield change recorded at that site.

2.6 Model for normal tissue complication probability

Analyses of normal tissue complication probability (NTCP) have commonly been based on a standard S-shaped dose response curve, of which the simplest in form is:

$$NTCP = \frac{1}{1 + (d / d_{50})^k} \quad (1)$$

Here, d_{50} is the dose at which on the average 50% of the cells would be killed; d is the dose delivered to the region of lung, and k is a factor that defines the steepness of dose response[10-11]. The resulting filtered and normalized datasets (bin dose value versus bin-averaged CT intensity changes) were used to solve (in a least-squares error sense) for the two

unknowns in the NCTP model of Equation 1 (the d_{50} and k parameters). The normalization step artificially alters the apparent slope (k) parameter value, but does not affect the d_{50} value.

2.7 Concurrent measurement of circulating cytokine levels

In patient #2, in addition to the pre- and post-treatment CT image acquisitions, blood samples were acquired at each corresponding time point to assess whether the dose response analysis could be used to address the interactions between the level of radiation sensitivity over time and the level of circulating cytokines. The circulating levels of the cytokines interleukin-1α (IL-1α), interleukin-8 (IL-8), transforming growth factor β (TGFβ) and monocyte-chemoattractant-protein-1 (MCP-1) were acquired at the same time points.

2.8 Evaluating robustness to registration error

To test the robustness of the model d_{50} and k parameters (Equation 1) to registration error, the data analysis for lesions 1, 3 and 5 in patient #1 was repeated but with induced registration errors of approximately 1, 2 and 3 mm. The in-plane pixel dimensions for the CT images used for this analysis were 0.94 mm, with slice thickness of 3 mm. The sensitivity analysis was accomplished for the 1 mm case by shifting the dose field by 1 pixel in +X direction (vertically in-plane), re-computing the d_{50} and k parameters, then shifting from the original configuration by 1 pixel in the –X direction and re-computing d_{50} and k. This was repeated for shifts in the +Y and –Y directions. The results for the 4 runs were then tallied to get the average and maximal change in the d_{50} and k values over all 4 runs. This was repeated for the 2 mm shift case. For the 3 mm shift case, shifts of 3 pixels in-plane and 1 slice (in the through-plane direction) were used. The process was repeated independently for treatment sites 1, 3 and 5.

3. RESULTS

3.1 Effect of treatment volume on dose response

The dose response approach was applied to the clinical treatment and follow-up data in patient #1 who was treated for five isolated lung metastases. For each lesion an independent treatment plan was constructed and executed (Figure 1). The cumulative radiation dose received over all five treatments was computed at each pixel. The dose-response results are shown in Figure 2. For each site, the treatment volume was computed as V_{80}, the volume of normal lung encompassed by the 80% isodose line. The smallest treatment volume was < 10 ml and at this site no pneumonitis was observed, even at the pixels receiving the highest dose of 50 Gy given at 5 Gy per fraction. Between 10 to 16 ml, the dose that causes a half-maximal change in Hounsfield units (d_{50}) is approximately 45 to 50 Gy. The dose response for these tumors was very steep, indicating a homogeneous response of functional lung units to the radiation damage. For irradiated lung volumes of over 16 ml, there is a more heterogeneous normal tissue response, evidenced by a less steep dose response curve. Thus, there is a volume effect that alters the radiation pneumonitic changes on chest CT, and there is also evidence of a lowering of tolerance as the field size increases. Using the data presented in Figure 2 and employing a standard linear regression analysis, we compute a normalized cross-correlation coefficient (r-value) between V_{80} and d_{50} of 0.65.

3.2 Time dependence of response

Radiation response also varies with time. As evident in Figure 3, the response curves in patient #1 are shifted to the right at 12 months post-treatment compared to 6 months. Figure 4 displays the same trends in patient #2 out to 16 months post PSRT. However, Figure 2 shows also the expected long-term progression of damage (left-ward shift in d_{50}) at the 23-month time point. The initial decrease in tissue density change may be due to "slow repair" in which tissues from outside of the irradiated volume grow into the affected region and replace lost tissue function and architecture. In contrast, an increase in the lung damage can be due to a slow relentless progression of inflammation. Changes over time have also been attributed to loss of specific "target" cells, where the temporal expression of radiation-induced damage, seen at early and late times, can be explained by different replication rates.

3.3 Effect of circulating cytokine levels on dose response

Concurrent blood samples were acquired at corresponding time points post-exposure. The circulating levels of the cytokines IL-1α, IL-8, TGFβ and MCP-1 were acquired at the same time points and are presented in Table 1. The r-

value between the time sequence of fitted d_{50} values and each cytokine is also given in Table 1. As seen in prior animal studies[12-14], a strong inverse correlation exists between the time pattern of tissue response and the temporal variation in circulating IL-1α and TGFβ levels, while MCP-1 shows a strong positive correlation. From the levels MCP-1 taken from the blood at 4 time points post-treatment and simultaneously sampled d_{50} values we computed a correlation r-value of 0.85 (Table 1).

3.4 Robustness to registration error

The results for the 3 mm registration shift analysis are shown in Figure 3. Table 2 gives the resulting percentage maximal changes in d_{50} and k for all lesions over all runs. The d_{50} index was found to be robust to registration errors up to 3 mm, with the largest change incurred in any of the runs in any of the lesions being < 5%. The k parameter was more sensitive to the induced registration error with percentage changes of up to 180% at the site with the smallest initial k value. Of particular importance, the changes in d_{50} due to registration error are an order of magnitude smaller than those changes in the dose response observed in Figures 1-3, including those changes that show a high correlation with circulating cytokines.

4. DISCUSSION

We have demonstrated a quantitative non-invasive *in vivo* method for measuring radiation dose-response in human lung tissue. The method is based on knowledge of the 3D dose delivery to the treatment site and tissue density information gathered from follow-up CT scans of the chest and was applied to patients treated for isolated lung lesions using high dose conformal radiation therapy. The analysis produced a sigmoid response curve for radiation dose exposure versus change in tissue density observed in CT Hounsfield units. Values were fit for the d_{50} index – the dose at which half maximal tissue density change is observed. The d_{50} index decreased with increasing treatment volume, as expected from prior experimental findings in animals. The d_{50} index increased with time from 3 to 12 months post-exposure, reflecting tissue repair, but then decreased from 12 months to 24 months suggestive of damage progression secondary to irreversible vascular deficiency. The time course of the dose-response also correlated well with circulating levels of key cytokines (IL-1α, TGFβ, MCP-1) known to be involved in the body's inflammatory response.

Image noise and limitations of clinical scanners to detect small changes in pixel intensities impose hard limits to the accuracy of the CT intensity change measurements. In our clinical experience, clinical CT scanners have a noise standard deviation of ~7 HU, while the intensity resolution of these clinical scanners is 3-5 HU. An assumption of our approach is that the measured tissue Hounsfield values are reproducible between imaging procedures and between different imaging devices. Because all clinical CT scanners used routinely at our institution undergo rigorous calibration checks at regular intervals, we expect this assumption to hold, at least to within ~10 HU tolerance. In our initial clinical study we found that the average pixel intensity of normal lung tissue is approximately -600 HU. The maximal intensity in radiation damaged lung tissue is approximately +50 HU, thus the range of pixel intensities of interest is ~650 HU. To fit a sigmoidal curve to the dose response data would require a minimum of 3 measurement points, however it would be unwise to attempt such a fit with less than 6 points. Over this range of ~650 HU, we require then an intensity resolution of ~110 HU, which is easily achievable in human subjects using conventional CT scanners.

Sigmoid dose-response models for tissue reactions have been used commonly in the past. However, in this analysis we are not measuring cellular reactions directly, but rather large-scale tissue density changes as observed under conventional CT imaging. A second assumption of our analysis approach is that tissue reaction to radiation as measured by changes in Hounsfield units is sufficiently consistent with the underlying cellular response to radiation that a sigmoid model is appropriate for CT-observed tissue density change due to radiation exposure at these high doses. As evident from the plots of the raw dose response data and the fitted curves in Figures 1 & 2, it would appear that the sigmoid model is appropriate enough to demonstrate the technique. Variants to the sigmoid NCTP model (Equation 1) have been presented in the literature, including one developed to study tumor control probability in humans[15]. We tested several formulations but all provided very similar fit to experimental data between the 10 and 90% NTCP levels. More complex models will be addressed in future work.

ACKNOWLEDGEMENTS

The authors wish to gratefully acknowledge funding support from the American Cancer Society (RSG-02-155-01-CCE), BrainLAB, AG, and the NIH (1R01CA109393-01:O'Dell)

REFERENCES

1. P. Okunieff, A. L. Petersen, A. Philip, M. T. Milano, A. W. Katz, L. Boros, and M. C. Schell, "Stereotactic Body Radiation Therapy (SBRT) for lung metastases," *Acta Oncol*, **45**, 808-817 (2006).
2. J. P. Williams, P. Keng, and R. M. Sutherland, "Basic Principles of Radiobiology," in *Clinical Oncology: a Multidisciplinary Approach for Physicians and Students*, P. Rubin, Ed., 8th ed. Philadelphia: WB Saunders, 2001.
3. E. L. Travis, "Organizational response of normal tissues to irradiation," *Seminars in Radiation Oncology*, **11**, 184-196 (2001).
4. Y. Chen, J. Williams, I. Ding, E. Hernady, W. Liu, T. Smudzin, J. N. Finkelstein, P. Rubin, and P. Okunieff, "Radiation pneumonitis and early circulatory cytokine markers," *Seminars in Radiation Oncology*, **12**, 26-33 (2002).
5. M. Kolb, P. Bonniaud, T. Galt, P. J. Sime, M. M. Kelly, P. J. Margetts, and J. Gauldie, "Differences in the fibrogenic response after transfer of active transforming growth factor-beta1 gene to lungs of "fibrosis-prone" and "fibrosis-resistant" mouse strains," *American Journal of Respiratory Cell & Molecular Biology*, **27**, 141-150 (2002).
6. M. S. Anscher, L. B. Marks, T. D. Shafman, R. Clough, H. Huang, A. Tisch, M. Munley, J. E. Herndon, 2nd, J. Garst, J. Crawford, and R. L. Jirtle, "Using plasma transforming growth factor beta-1 during radiotherapy to select patients for dose escalation," *Journal of Clinical Oncology*, **19**, 3758-3765 (2001).
7. T. E. Schultheiss, "The controversies and pitfalls in modeling normal tissue radiation injury/damage," *Seminars in Radiation Oncology*, **11**, 210-214 (2001).
8. H. Liu, Y. Yu, M. C. Schell, W. G. O'Dell, R. Ruo, and P. Okunieff, "Optimal marker placement in photogrammetry patient positioning system," *Med Phys*, **30**, 103-110 (2003).
9. W. O'Dell, M. Schell, and P. Okunieff, "Margin optimization for fractioned breath-hold radiation therapy," AAPM 44th Annual Meeting, Montreal, Quebec, Canada, July 2002.
10. J. C. Theuws, S. H. Muller, Y. Seppenwoolde, S. L. Kwa, L. J. Boersma, G. A. Hart, P. Baas, and J. V. Lebesque, "Effect of radiotherapy and chemotherapy on pulmonary function after treatment for breast cancer and lymphoma: A follow-up study," *Journal of Clinical Oncology*, **17**, 3091-3100 (1999).
11. A. Niemierko and M. Goitein, "Calculation of normal tissue complication probability and dose-volume histogram reduction schemes for tissues with a critical element architecture," *Radiotherapy & Oncology*, **20**, 166-176 (1991).
12. M. S. Anscher, F. M. Kong, L. B. Marks, G. C. Bentel, and R. L. Jirtle, "Changes in plasma transforming growth factor beta during radiotherapy and the risk of symptomatic radiation-induced pneumonitis," *International Journal of Radiation Oncology, Biology, Physics*, **37**, 253-258 (1997).
13. M. S. Anscher, F. M. Kong, K. Andrews, R. Clough, L. B. Marks, G. Bentel, and R. L. Jirtle, "Plasma transforming growth factor beta1 as a predictor of radiation pneumonitis," *International Journal of Radiation Oncology, Biology, Physics*, **41**, 1029-1035 (1998).
14. I. Baumer, G. Zissel, M. Schlaak, and J. Muller-Quernheim, "Soluble intercellular adhesion molecule 1 (sICAM-1) in bronchoalveolar lavage (BAL) cell cultures and in the circulation of patients with tuberculosis, hypersensitivity pneumonitis and sarcoidosis," *European Journal of Medical Research*, **3**, 288-294 (1998).
15. P. Okunieff, D. Morgan, A. Niemierko, and H. D. Suit, "Radiation dose-response of human tumors," *International Journal of Radiation Oncology, Biology, Physics*, **32**, 1227-1237 (1995).

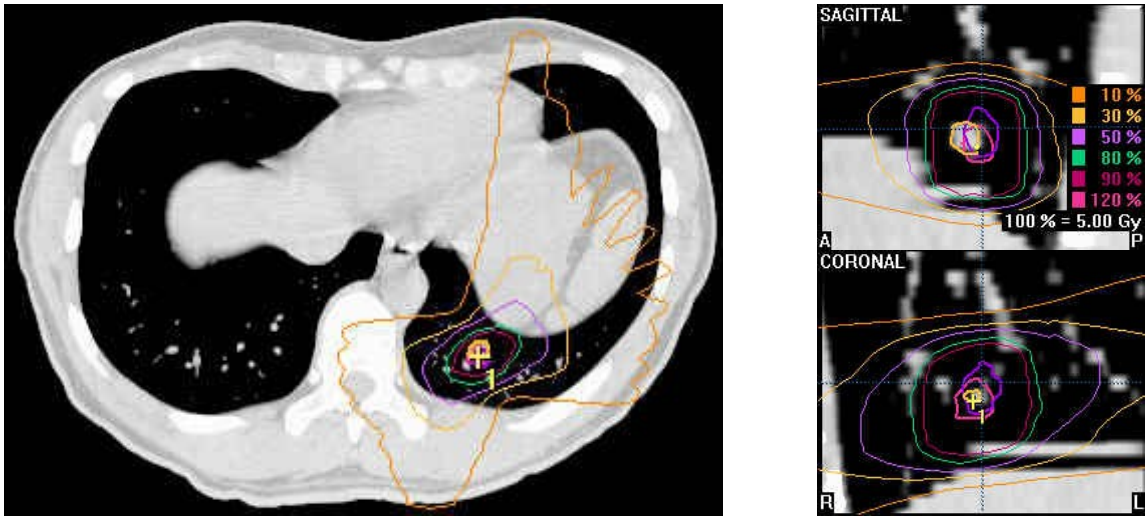

Figure 1. Radiation isodose contours for the treatment of Lesion 1 in patient #1. At 14 mm, this had the largest diameter of the five lesions treated. 100% dose = 5 Gy per fraction; 50 Gy total. The yellow cross and central orange outlines were manually defined to mark the location of the tumor centroid. The central purple and pink contours mark the location of the tumor in two previous CT image acquisitions: purple = pretreatment; pink = 3rd day; orange = 6th day. The surrounding contours (red, green, purple, yellow & orange) are the isodose contours in the treatment plan. As demonstrated by the dose conformity of the contours around the target at each day, setup reproducibility and dosimetry was as per prescription and resulted in a lethal dose delivered to the tumor and surrounding space.

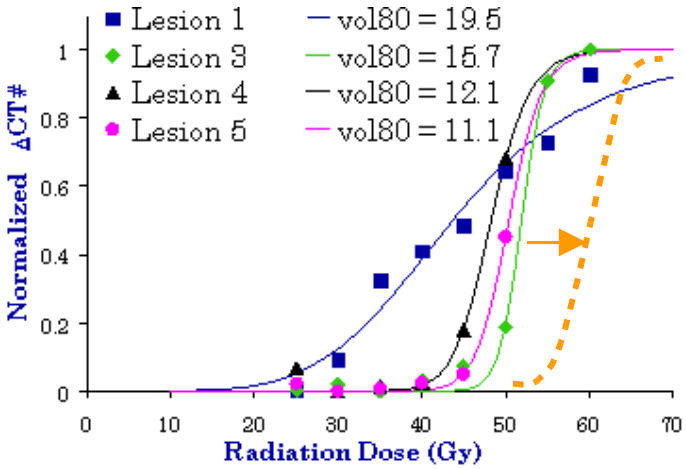

Figure 2. Dose response curves for the 5 treatment sites in patient #1 at 6 months post-treatment. For each site vol_{80} [ml] is the volume of normal lung tissue included in the 80% isodose volumes. The symbols are the measured data. The curves are fitted to Equation 1. All lesions were treated to 50 Gy at the 100% isodose over 10 fractions. Lesion 2 had the smallest volume of < 10 ml and had no associated Hounsfield unit changes. This is represented in the plot by the conceptual toxicity curve (orange dotted line) that is shifted to the right beyond our maximum applied doses. The larger volumes of radiation caused lung changes at a lower dose than the smaller treatment volumes. There is also an increased heterogeneity of response indicated by the shallow dose response for the largest treatment site (Lesion 1 – dark blue curve).

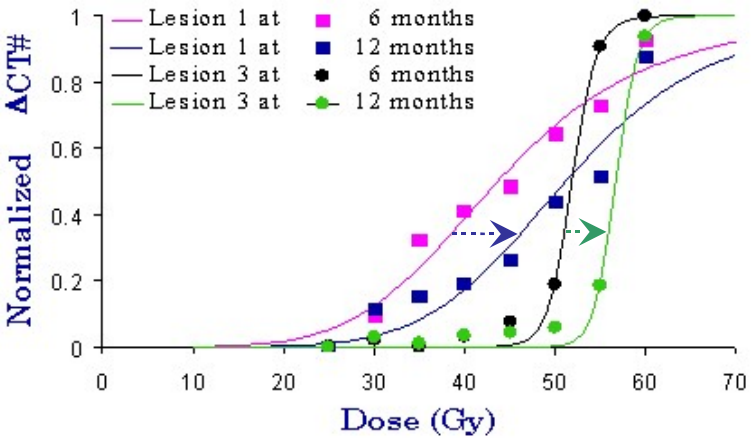

Figure 3. Shift in the dose response curves from 6 to 12 months post-treatment for the two largest treatment volumes (for Lesions 1 and 3) in the dataset shown in Figure 1. The 6-month data shows a lower d_{50} than the 12-month data for this patient, indicated by a right-ward shift of the plots, suggesting partial recovery during the interval.

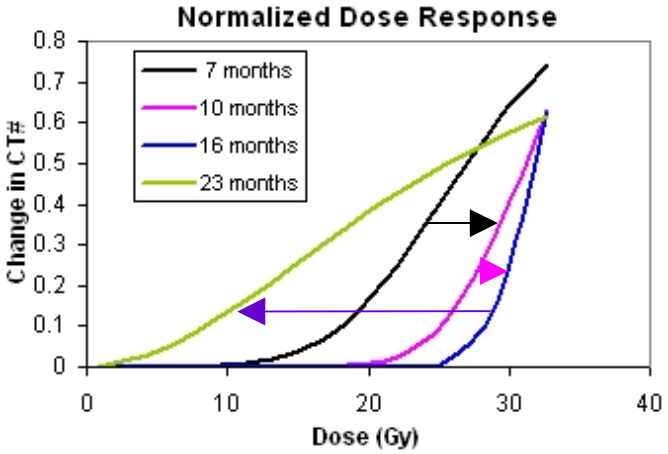

Figure 4. Fitted dose response curves for a patient (patient #2) who was treated for a single 18 mm diameter lung lesion. Shown are the data corresponding to follow-up images that were acquired at 7, 10, 16 and 23 months post treatment. These follow-up times are those associated with blood plasma cytokine measurements acquired in the same subject; presented in Table 1. At the 23-month time point, the slope of the tissue response curve exhibited approximately a 1%/Gy increase.

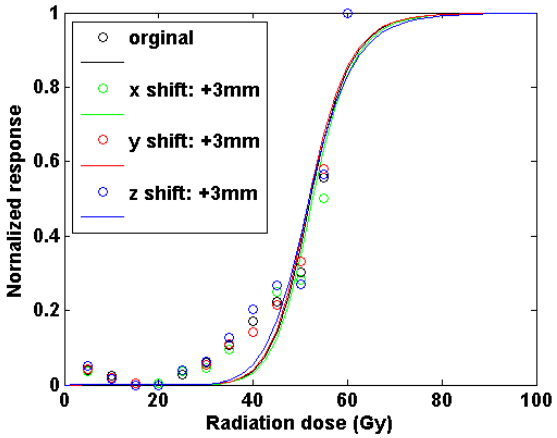

Figure 5. Plots of the dose-response data and the associated fitted curves patient #1 following induced registration shifts of 3 mm in each of the X, Y (in-plane) and through-plane (Z) directions. The fitting was performed using the sigmoidal formulation of Equation 1. The maximal change in the fitted k parameter was 10% and that for the fitted d_{50} value was < 1% for this treatment site, as shown in Table 2.

Table 1. Comparison between the fitted d_{50} dose-response values and blood cytokine measurements at the same time points. As predicted by previous animal studies, the temporal variations in circulating IL-1α and TGFβ show a strong inverse correlation with patterns of tissue response over time, while MCP-1 shows a strong positive correlation.

Date	7 mo	10 mo	16 mo	23 mo	
fitted d_{50}	26.98	31.04	31.79	25.70	r-value
IL-1α(pg/ml)	3.57	0.00	2.04	5.33	-0.87
TGFβ (pg/ml)	22.5	19.7	12.5	24.7	-0.89
IL-8 (pg/ml)	24.3	10.8	12.6	11.4	-0.39
MCP-1 (pg/ml)	198.9	538.6	682.1	367.5	+0.85

Table 2. Sensitivity of the d_{50} and k parameters (Equation 1) to simulated 3 mm registration error for Lesions 1, 3 & 5 in patient #1.

	Lesion 1	Lesion 3	Lesion 5
reference d_{50}	52.12	51.67	42.10
Δd_{50} max	0.9%	4.4%	2.7%
reference k	12.31	6.99	10.7
Δk max	10%	180%	12%